NANO LETTERS

LETTER

pubs.acs.org/NanoLett

# Photoluminescence from Inner Walls in Double-Walled Carbon Nanotubes: Some Do, Some Do Not

Sungwoo Yang,[†] Ashley N. Parks,[‡] Stacey A. Saba,[†] P. Lee Ferguson,[*,‡,§] and Jie Liu[*,†]

[†]Department of Chemistry, [‡]Nicholas School of the Environment, and [§]Department of Civil and Environmental Engineering, Duke University, Durham, North Carolina, 27708, United States

Supporting Information

**ABSTRACT:** Double-walled carbon nanotubes (DWNTs) have recently been recognized as important members in the carbon nanotube family because they are expected to have certain unique properties. For example, DWNTs are expected to replace single-walled carbon nanotubes (SWNTs) in biomarker applications and optoelectronics if the observed luminescence from DWNTs can be verified. However, due to unavoidable byproducts, such as SWNTs, optical properties of DWNTs still remain controversial. There is an ongoing debate concerning the ability of DWNTs to exhibit photoluminescence (PL). In this report, we aim to clearly resolve this debate through the study of carefully separated DWNTs. DWNTs were successfully separated from SWNTs using density gradient ultracentrifugation. Here we clearly show that light is emitted from the inner wall of DWNTs; however, the intensity of the emission is significantly quenched. Interestingly, it was found that a very narrow range of diameters of the inner walls of DWNTs is required for PL to be observable. All other diameters led to complete PL quenching in DWNTs. In short, we have shown that both sides of the debate are correct under certain situations. The real answer to the question is that some DWNTs do emit light but most DWNTs do not.

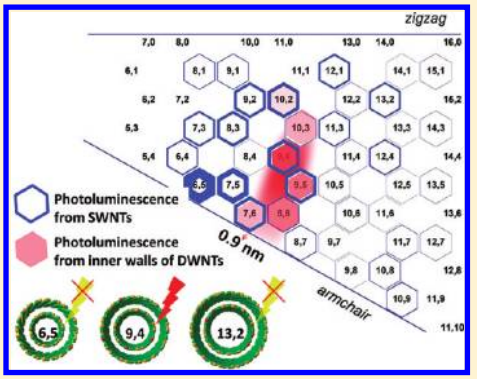


**KEYWORDS:** Double-walled carbon nanotubes, separation, sorting, photoluminescence, density gradient ultracentrifugation

Double-walled carbon nanotubes (DWNTs) have recently been recognized as important members in the carbon nanotube (CNTs) family because they are expected to have certain properties superior to single-walled carbon nanotubes (SWNTs) or multiwalled carbon nanotubes (MWNTs). For example, DWNTs are expected to replace SWNTs in biomarker applications[1] and optoelectronics,[2] if the observed luminescence from DWNTs in these earlier reports can be verified. However, due to unavoidable byproducts, such as SWNTs and MWNTs, optical properties of DWNTs still remain controversial. There is an ongoing debate in the research field concerning the ability of DWNTs to exhibit photoluminescence (PL). Okazaki et al. reported that a decrease in the interlayer distance enhances the interaction between the inner and outer shells, resulting in a higher degree of PL quenching.[3] Tsyboulski et al. also concluded that near IR emission from their DWNTs enriched samples resulted from SWNTs impurities rather than from the inner shells of DWNTs.[4] In addition, Koyama et al. found that the relative intensity of steady-state luminescence from the inner walls in DWNTs is ~700 times weaker than that from SWNTs.[5] On the other hand, Kishi et al. reported that light is emitted from the inner tubes of a majority of DWNTs (90%),[6] and Iakoubovskii et al. demonstrated DWNTs exhibit strong PL in their experiments.[7] Furthermore, Hertel et al. showed evidence of PL from the inner walls of DWNTs and their red-shift of exciton transition.[8] More recently, Muramatsu observed bright PL from the inner walls of DWNTs synthesized using the peapods approach.[9] These seemingly contradictory observations fueled a heated debate in the research field on whether DWNTs can fluoresce at all.

In this report, we aim to clearly resolve this debate through the study of carefully separated DWNTs. DWNTs were successfully separated from SWNTs using density gradient ultracentrifugation (DGU). Here we clearly show that light is emitted from the inner wall of DWNTs; however, the intensity of the emission is significantly quenched. Interestingly, it was found that a very narrow range of diameters of the inner walls of DWNTs is required for PL to be observable. All other diameters led to complete PL quenching in DWNTs. In short, we have shown that both sides of the debate are correct under certain situations. The real answer to the question is that some DWNTs do emit light but most DWNTs do not. As is true for SWNT, the PL properties of DWNTs are highly dependent on their helicity.

Cobalt (Co) and molybdenum (Mo) were used as catalysts, and titanium silicalite zeolite (TS-1) was used as the catalyst support, because its specific porosity promotes DWNT production. Specifically, Co, Mo, and zeolites with a specific molar ratio (Co:Mo = 6:1) were dissolved into methanol and heated on a hot plate to evaporate all of the solvents. The resulting solid-phase mixture was annealed at 530 °C to remove residual organic

**Received:** July 27, 2011
**Revised:** August 28, 2011

   dx.doi.org/10.1021/nl2025745 | *Nano Lett.* XXXX, XXX, 000–000

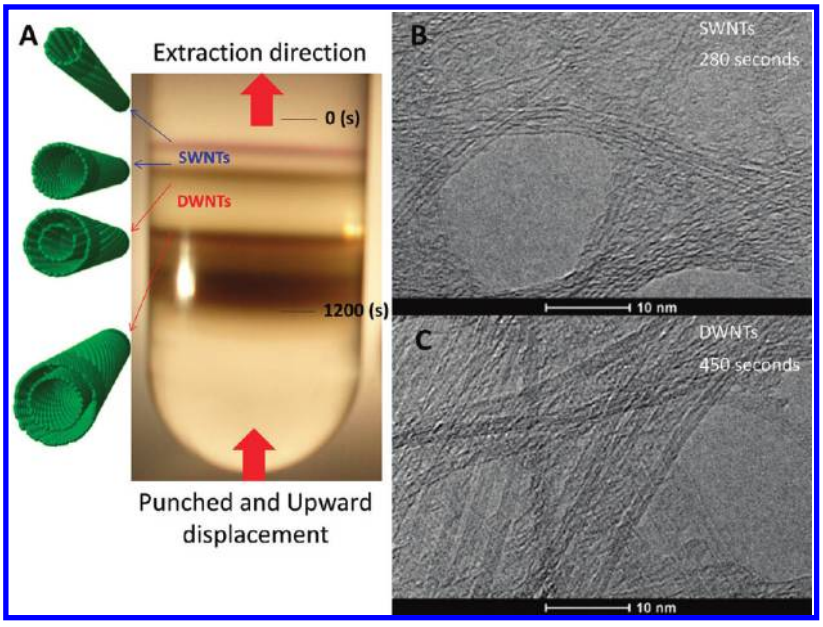


**Figure 1.** (A) Digital image of separated layers of CNTs using DGU method. All layers are labeled, and the time scale shown in the middle is corresponding to the time in spectral plots. After 1200 s, all layers of nanotubes are extracted from the centrifuge tube. (B) TEM image of samples extracted at 280 s, in SWNT region. (C) TEM image of samples extracted at 450 s, in DWNT region.

impurities. DWNTs were successfully synthesized at 900 °C with ethanol as the precursor carried by argon. The raw DWNTs were burned at 550 °C for 5 h in air to remove amorphous carbon impurities, and hydrofluoric acid was used to remove zeolite supports and metal seeds.

A 5 mL linear density gradient was created directly in the centrifuge tube with OptiPrep 60% w/v iodixanol (Sigma-Aldrich, Inc.) using a linear gradient maker (SG 15 gradient maker, Hoefer, Inc.). It ranged from 22.5% w/v iodixanol and 2% w/v sodium cholate (SC) to 7.5% w/v iodixanol and 2% w/v SC. The gradient was added on top of a 1.5 mL underlayer of 60% w/v iodixanol 2% SC. An aliquot of the precentrifuged DWNT suspension was mixed with 60% w/v iodixanol to create a final iodixanol concentration of 20% w/v, and 1.0 mL of this suspension was added 5/6 from the top of the gradient at 0.1 mL/min using a syringe pump (KD Scientific). Approximately 4.5 mL of 2% w/v SC was added to fill the remainder of the tube. This method was adapted from the method by Arnold et al.[10]

The samples were ultracentrifuged for 12 h at 22 °C and 41 000 rpm (Beckman-Coulter SW41 rotor). Upon completion, the samples were fractionated utilizing upward displacement at 0.3 mL/min with Fluorinert FC-40 (Sigma-Aldrich) as the dense chase medium. Fractionation was performed by placing the centrifuge tube in a custom built fractionator, where the bottom of the centrifuge tube was pierced with a 25 gauge needle (BD 305122), and the top was sealed and connected to the inflow tube of the flow cell. This tube was connected to a custom fluorometer flow cell (Z-dimension 9 mm, nominal volume 40 $\mu$L, Starna Cells, Inc.), where the near-infrared fluorescence (NIRF) and absorbance of the samples were measured as they were fractionated. Each fraction was then collected from the outflow tube of the flow cell every 10 s. Teflon PFA tubing with I.D. 0.020 in. and O.D. 1/16 in. (IDEX, part #1500) was used as the inflow and outflow tubing of the flow cell. NIRF and absorbance were measured using a NS1 Nanospectralyzer (Applied NanoFluorescence, LLC). The samples were excited with three lasers (638, 691, and 782 nm), and the resulting emission was detected from 880 to 1580 nm with an InGaAs array detector cooled to −18 °C. Fluorescence and absorbance were measured continuously until the entire sample was fractionated and passed through the flow cell. One set of fluorescence and absorbance measurements was taken every 10 s. The measurement parameters were as follows: 85 ms fluorescence integration time with 8 spectral averages for each excitation wavelength, and 60 ms absorbance integration time with 1 spectral average. Further details on fractionation method design and optimization along with a photograph of the customized fractionation apparatus can be found in the Supporting Information.

After purifying synthesized CNTs, high-resolution transmission electron microscopy (TEM) was used to determine CNT species by counting the numbers of SWNTs, DWNTs, and thin MWNTs, as shown in Figure S1, Supporting Information. It is found that major species of as-grown CNTs were DWNTs (77%), and the other type of CNTs, such as SWNTs (9%) and thin MWNTs (14%), coexisted together. In our studies, we have used density gradient ultracentrifugation (DGU)[10] to separate DWNTs from other CNTs. The centrifuge tube shown in Figure 1 illustrates separated layers, each containing different species of CNTs. Upon completion of DGU, the layers were fractionated utilizing upward displacement[11] with Fluorinert FC-40 (Sigma-Aldrich) as the dense chase medium. The layers were pumped from the centrifuge tube through a custom flow cell mounted in an NS1 NanoSpectralyzer (Applied NanoFluorescence, Houston, TX) where NIR absorption and PL spectra were measured. In order to decrease the mixing of adjacent layers and minimize peak aliasing, the flow rate was optimized by calculating the Nyquist limit for spectral acquisition. Details can be found in the Supporting Information. A syringe pump (KD Scientific) was used to achieve a stable flow rate, and time (in seconds) was recorded during the extraction and plotted as the $x$-axis in Figure 2. There was a clear separation of the PL from SWNT and DWNT species at 320 s, as denoted by the resolution of the


dx.doi.org/10.1021/nl2025745 |*Nano Lett.* XXXX, XXX, 000–000

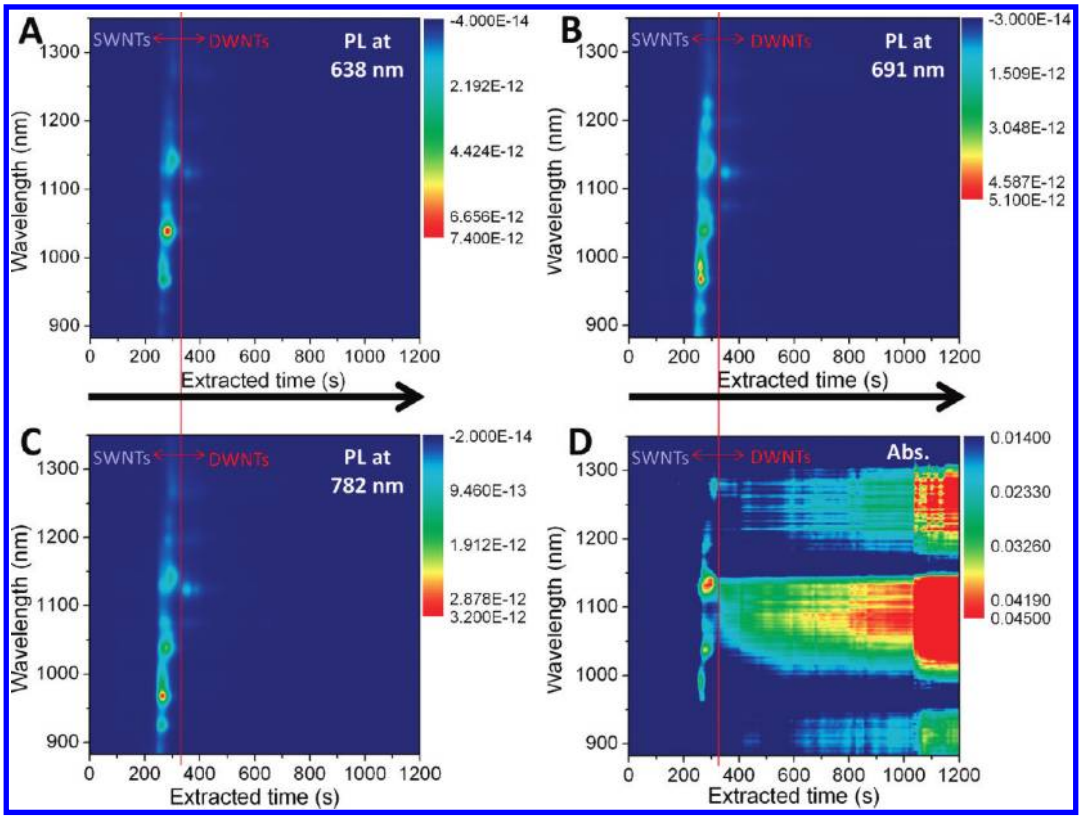


**Figure 2.** PL maps from separated SWNTs and DWNTs excited with: (A) 638, (B) 691, and (C) 782 nm lasers. *X*-axis is time frame in seconds, *Y*-axis is the emission wavelength in nm, and (D) shows the absorption map with the same time frame. The color represents signal intensity in both PL (nW/cm) and absorption spectra using the presented color scale.

two (9, 4) elution profiles as shown in Figure 2A. Because PL and absorption spectra were simultaneously recorded, all *x*-axes in Figure 2 represent the same time frame. The *y*-axis represents the wavelength of the PL or absorption spectroscopy. In all of these maps, the color represents the intensity of the peaks of the PL and absorption using the presented color scale.

The intensity of absorption peaks is directly proportional to CNT concentration in the DGU-separated suspensions.[12] As shown in Figure 2D, we detected the start of the first CNT layer at approximately 250 s after initiation of DGU tube displacement. Full displacement of CNTs was completed in 1200 s. Samples were collected into small vials every 10 s, corresponding to the total time per set of absorption and PL measurements. These samples were then characterized using HRTEM. It should be noted that DWNTs were observed only after 320 s in the extraction time frame. TEM images in Figure 1 indicated typical SWNTs (top) and DWNTs (bottom) isolated using this strategy. Rance et al. recently reported no correlation between structural parameter (diameter, length, and number of concentric layers) and extinction coefficients for all nanotube samples they studied.[13] Therefore, the absorption spectra in Figure 2D indicates that as-synthesized CNTs include more DWNTs compared to SWNTs because the intensity of the absorption from DWNT region is much higher than that of SWNTs. This was confirmed by TEM (Figure S1, Supporting Information), which indicated a higher numerical density of DWNT relative to SWNT. As is evident from the PL plots in Figure 2, a strong, CNT-derived PL signal was detected at approximately 250 s, corresponding to the time when SWNTs were extracted from the centrifuge tube. We carefully analyzed the ($n$, $m$) chirality of these SWNTs based on their PL spectra and found that these SWNTs were sorted by their diameter, as shown in Figure 3A and B and will be described. On the other hand, the PL signals from the DWNTs samples extracted around 1000 s were far less intense, in spite of the finding that the concentration of DWNTs in these sections was higher than the concentration of SWNTs in earlier extracted sections. Therefore, simultaneous comparison between PL and absorption map clearly demonstrated PL quenching of DWNTs. In fact, we could only detect PL signals from DWNTs with inner walls falling within a very narrow range of diameters, as discussed below.

Figure 3 shows some important PL peaks isolated from the SWNT region (240−300 s in the extraction process) and DWNT region (after 330 s). We utilized an NS1 NanoSpectralyzer (Applied NanoFluorescence) to collect PL and absorption spectra as well as to characterize ($n$,$m$) chirality and diameter distributions of CNTs. As expected, SWNTs were sorted by their diameter during DGU. For example, the major species was (8,3) in the section around 260 s; (7,5) in the section around 280 s; and (7,6) in the section around 300 s. The corresponding theoretical diameters of these nanotubes are 0.782 nm, 0.829 nm and 0.895 nm. In addition, the smallest nanotube we detected was (8,1) with a diameter of 0.678 nm, and the largest one was (10,9) with a diameter of 1.307 nm based on PL analysis. This diameter range of SWNTs was well matched with Raman analysis of dried SWNTs film using the extracted sections of CNTs suspensions (240 s ∼ 300 s) as shown in Figure S3 in the Supporting Information.


dx.doi.org/10.1021/nl2025745 |*Nano Lett.* XXXX, XXX, 000–000

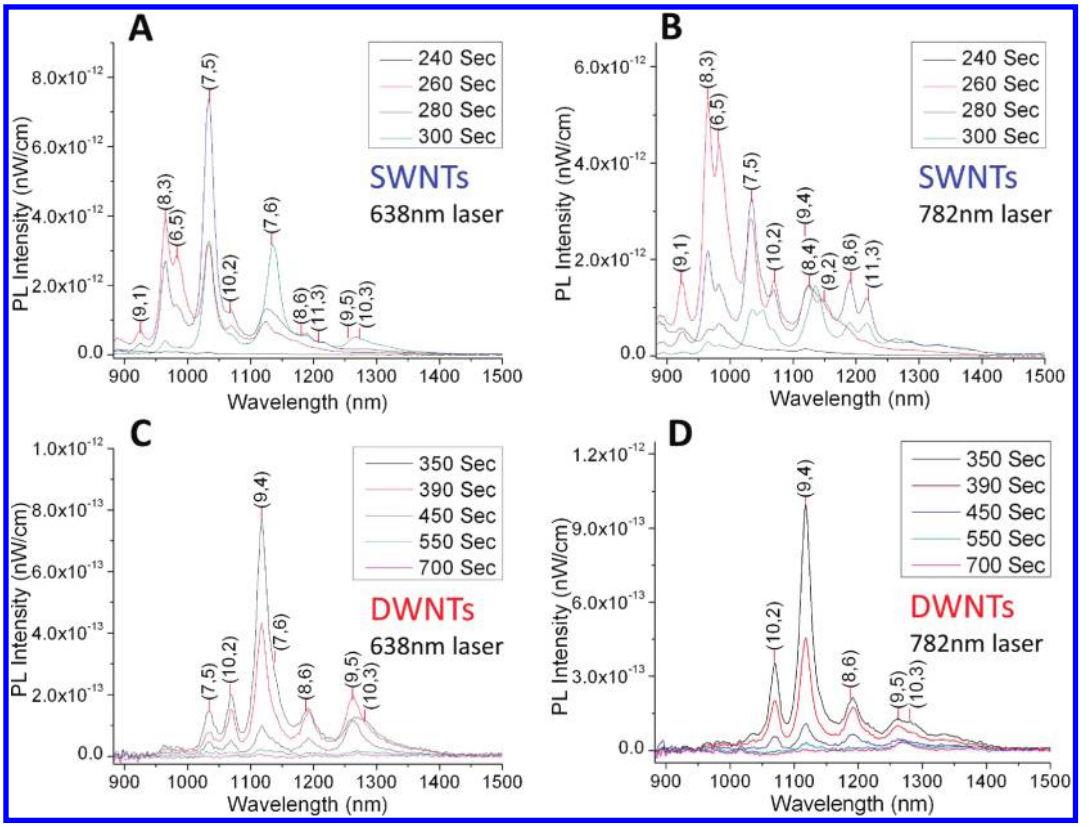


**Figure 3.** PL from DGU separated SWNTs excited with: (A) 638 and (B) 782 nm lasers and DWNTs layers excited with: (C) 638 and (D) 782 nm lasers. *Y*-axis represents intensity, and *x*-axis represents emission wavelength (nm). For excitation, 638 and 782 nm wavelength lasers were used . Samples isolated prior to 320 s correspond to the SWNTs region and after 320 s to the DWNTs region.

**Table 1. Typical $(n,m)$ Chirality Associated with the Inner Walls of DWNTs Found in PL from DWNTs Region Using 638 and 782 nm Lasers**

| $(n,m)$ | $E_{11}$ (nm) | diameter (nm) | angle (°) |
|---|---|---|---|
| (10,2) | 1069 | 0.884 | 8.95 |
| (9,4) | 1118 | 0.916 | 17.48 |
| (7,6) | 1138 | 0.895 | 27.46 |
| (8,6) | 1188 | 0.966 | 25.29 |
| (9,5) | 1263 | 0.976 | 20.63 |
| (10,3) | 1281 | 0.936 | 12.73 |

More interestingly, there was a significant difference in the PL spectra of SWNT and DWNT regions. We found more diverse $(n,m)$ distribution in the SWNT region than in the DWNT region. Only a few peaks were observed from DWNT region. Table 1 summarizes these peaks, showing $(n,m)$ chirality with theoretical diameter and chiral angle.

In this study, one of the most challenging questions to answer is to ensure that PL detected in the DWNT region originated from the inner walls of DWNTs rather than SWNT impurities. Although sorted CNT layers were extracted from the centrifuge tubes using an optimized extraction rate based on Nyquist limit calculations, there was always a small possibility of the existence of SWNTs in the DWNTs region. As summarized below, we have shown using several experimental strategies that PL from the DWNT region (i.e., after 320 s) originates from the inner walls of DWNTs rather than from SWNT impurities.

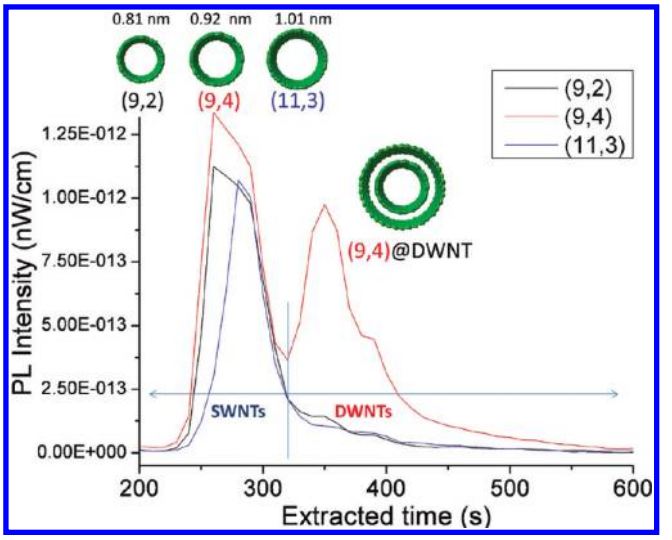


**Figure 4.** PL intensity comparison between select $(n,m)$ nanotubes. The PL wavelength corresponding specific $(n,m)$ CNTs are 1152, 1120, and 1212 nm for (9,2) (black line), (9,4) (red line), and (11,3) (blue line), respectively. The images of CNTs were created by nanotube coordinate generator from http://www.photon.t.u-tokyo.ac.jp/~maruyama/wrapping3/wrapping.html. Only the (9,4) nanotube strongly fluoresced in DWNTs region, while the PL from the other two nanotubes were weak.

The results of the first set of experimental results aimed at such demonstration are shown in Figure 4. We observed the PL


dx.doi.org/10.1021/nl2025745 |*Nano Lett.* XXXX, XXX, 000–000

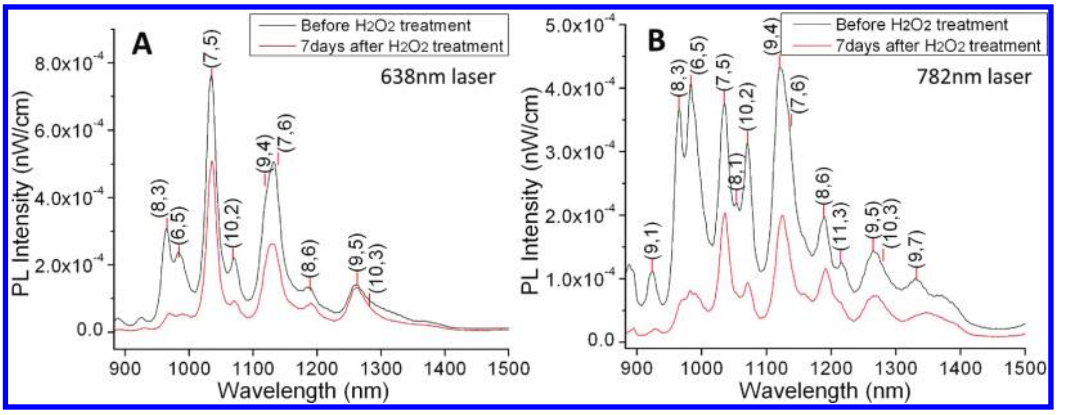


**Figure 5.** PL intensity comparison of the precentrifuged CNT suspension before (black) and after (red) $H_2O_2$ treatment. Left (A) and right (B) are PL with 638 and 782 nm wavelength laser.

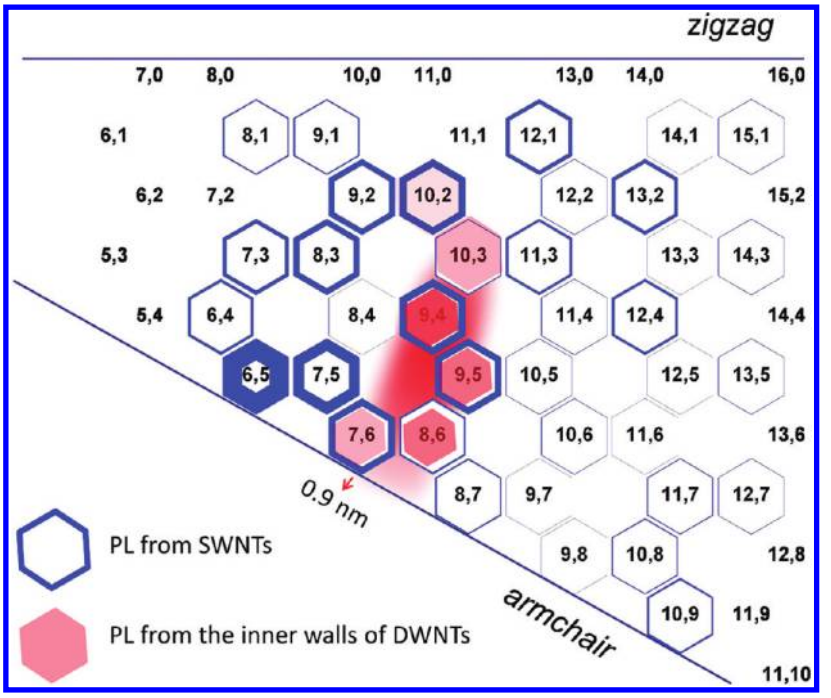


**Figure 6.** The $(n,m)$ chirality map of the DGU separated SWNTs and DWNTs. Relative abundance is denoted by line thickness (SWNTs) or color gradient (DWNTs).

intensity change of the (9,2), (9,4), and (11,3) nanotubes as a function of DGU displacement time. As expected, the highest PL intensity of (9,2) nanotube was observed first followed by (9,4) and then (11,3) in the SWNT region, indicating that SWNTs were sorted by their diameter. However, a strong PL signal was detected again only from the (9,4) nanotube around 350 s (within the DWNT region). If the PL signal in the DWNT region was derived from SWNT impurities, then the largest (11,3) among these three nanotubes should have had a higher probability to be found in this higher buoyant density region due to its larger diameter. Furthermore, the intensities of the peaks from (9,2) and (9,4) nanotubes are similar to each other, but only (9,4) nanotubes were observed in the DWNTs region. If the PL signals in the DWNT regions were derived from SWNT impurities, then their intensity should have been similar in both regions. This comparison suggests that the emission from (9,4) nanotubes in the DWNT region was derived from inner tubes of DWNTs.

More importantly, we have studied the effect of quenching on the overall intensity of PL from unseparated nanotube suspensions to further confirm the existence of PL from DWNTs with specific inner tubes. Recently, McDonald et al. reported that the addition of $H_2O_2$ to suspensions of SWNTs results in PL quenching from all nanotubes except the (7,5) nanotubes, allegedly due to the protecting effect by sodium cholate surfactants from $H_2O_2$.[14] Here we performed a similar experiment on the mixture of SWNTs and DWNTs (Supporting Information). Figure 5 shows PL from the suspension of CNTs before and after $H_2O_2$ treatment. From the data shown in Figure 5, (10,2), (9,4), (7,6), (8,6), (9,5), and (10,3) nanotubes were detected after $H_2O_2$ treatment for 7 days in addition to the (7,5) nanotube observed in the referencing reports. The insensitivity of the PL


dx.doi.org/10.1021/nl2025745 |*Nano Lett.* XXXX, XXX, 000–000

from these types of nanotubes is a good indication that they are being protected from $H_2O_2$ attack. It is also worth noting that all of these six types of nanotubes were observed in the DWNT region in Figure 3C and D. This result provides strong evidence that PL observed from all of these six types of nanotubes originated from the inner walls of DWNTs. This conclusion is also supported by Figure S6, Supporting Information, when sodium dodecyl sulfate (SDS) is used to stabilize the nanotube suspension. In addition, it is worthwhile to note that, in addition to the PL depression from small-diameter nanotubes, such as (9,1), (8,3), and (6,5), we have also observed the PL depression from large-diameter nanotubes, such as (11,3) and (9,7), as shown in Figure 5.

Figure 6 illustrates the $(n,m)$ chirality map on a graphene lattice, indicating the population of each $(n,m)$ nanotube based on PL analysis using the NS1 NanoSpectralyzer software. The thickness of the blue hexagon edges represents PL peak intensity detected from SWNTs, and red color fill represents PL peak intensity from DWNTs. It is obvious that fewer $(n,m)$ possibilities were detected from DWNTs region compared to that of SWNTs. It is worthwhile to note that the average diameter of these $(n,m)$ nanotubes from the inner walls of DWNTs was approximately 0.929 nm and that all of these $(n,m)$ nanotubes have a relatively large chiral angle. This observation agrees well with reports by Bachilo et al.,[15] reporting that the highest PL intensity is expected from SWNTs with 0.930 nm diameter and large chiral angles among all SWNTs due to the combinations of trigonal warping and excitonic effects. These results pointed out a possibility that in DWNTs, only those inner walls with highest theoretical PL intensity could overcome the quenching effect from the outer walls. Therefore, for applications of biomarkers or photoelectronic devices, only DWNTs with certain inner walls can be used if PL is the method of detection. All other DWNTs could not be detected by PL due to strong quenching effects from the outer walls. Our conclusion can be used to explain some of the contradicting results in previous reports on fluorescence from the inner walls of DWNTs.[3−9]

In summary, we have presented a comprehensive optical characterization of purified DWNTs aimed at solving an ongoing debate in the research field concerning whether the inner walls of DWNTs produce NIR photoluminescence. In the experiments, DWNTs were separated by the DGU method. TEM, absorption, PL and Raman spectra demonstrated that mixtures of synthesized CNTs were successfully sorted by their number of side walls and diameter. We measured bimodal PL excitation maps and compared DWNTs and SWNTs. The results demonstrate significant PL quenching in DWNTs. However, PL from the inner wall of certain DWNTs was observed. Careful analysis of the data showed that only DWNTs with inner walls approximately 0.93 nm in diameter and with high chiral angles could be observed in the PL experiments. This observation can explain the seemingly contradictory results in the literature on DWNT photoluminescence. The final answer to the question on whether DWNTs photoluminesce is that some do and some do not. The PL emissions from DWNTs are highly dependent on their helicity. This observation provides strong insight and guidance on the application of DWNTs in biomarkers and photoelectronics.

## ■ ASSOCIATED CONTENT

**Ⓢ Supporting Information.** Details on fractionation method design and optimization along with a photograph of the customized fractionation apparatus. This material is available free of charge via the Internet at http://pubs.acs.org.

## ■ AUTHOR INFORMATION

**Corresponding Author**

*E-mail: j.liu@duke.edu; lee.ferguson@duke.edu.

## ■ ACKNOWLEDGMENT

We thank Xin Su and Xin Zhan for constructive discussions. This work was supported by funds from Duke University and from the National Science Foundation (NSF) and the Environmental Protection Agency (EPA) under NSF Cooperative Agreement EF-0830093 through the Center for the Environmental Implications of NanoTechnology (CEINT). S.A.S. is supported by NSF through a REU program at Duke University. The authors also acknowledge Professor Shigeo Maruyama for making the nanotube coordinate generator software available for public use.

## ■ REFERENCES

(1) Heller, D. A.; Baik, S.; Eurell, T. E.; Strano, M. S. *Adv. Mater.* **2005**, *17*, 2793.
(2) Itkis, M. E.; Borondics, F.; Yu, A.; Haddon, R. C. *Science* **2006**, *312*, 413.
(3) Okazaki, T.; Bandow, S.; Tamura, G.; Fujita, Y.; Iakoubovskii, K.; Kazaoui, S.; Minami, N.; Saito, T.; Suenaga, K.; Iijima, S. *Phys. Rev. B* **2006**, *74*, 153404.
(4) Tsyboulski, D. A.; Hou, Y.; Fakhri, N.; Ghosh, S.; Zhang, R.; Bachilo, S. M.; Pasquali, M.; Chen, L.; Liu, J.; Weisman, R. B. *Nano Lett.* **2009**, *9*, 3282.
(5) Koyama, T.; Asada, Y.; Hikosaka, N.; Miyata, Y.; Shinohara, H.; Nakamura, A. *ACS Nano*, article ASAP.
(6) Kishi, N.; Kikuchi, S.; Ramesh, P.; Sugai, T.; Watanabe, Y.; Shinohara, H. *J. Phys. Chem. B* **2006**, *110*, 24816.
(7) Iakoubovskii, K.; Minami, N.; Ueno, T.; Kazaoui, S.; Kataura, H. *J. Phys. Chem. C* **2008**, *112*, 11194.
(8) Hertel, T.; Hagen, A.; Talalaev, V.; Arnold, K.; Hennrich, F.; Kappes, M.; Rosenthal, S.; McBride, J.; Ulbricht, H.; Flahaut, E. *Nano Lett.* **2005**, *5*, 511.
(9) Muramatsu, H.; Hayashi, T.; Kim, Y. A.; Shimamoto, D.; Endo, M.; Meunier, V.; Sumpter, B. G.; Terrones, M.; Dresselhaus, M. S. *Small* **2009**, *5*, 2678.
(10) Arnold, M. S.; Green, A. A.; Hulvat, J. F.; Stupp, S. I.; Hersam, M. C. *Nat Nano* **2006**, *1*, 60.
(11) Graham, D. J. *Biological Centrifugation*; Garland Science: New York, 2001.
(12) Jeong, S. H.; Kim, K. K.; Jeong, S. J.; An, K. H.; Lee, S. H.; Lee, Y. H. *Synth. Met.* **2007**, *157*, 570.
(13) Rance, G. A.; Marsh, D. H.; Nicholas, R. J.; Khlobystov, A. N. *Chem. Phys. Lett.* **2010**, *493*, 19.
(14) McDonald, T. J.; Blackburn, J. L.; Metzger, W. K.; Rumbles, G.; Heben, M. J. *J. Phys. Chem. C* **2007**, *111*, 17894.
(15) Bachilo, S. M.; Strano, M. S.; Kittrell, C.; Hauge, R. H.; Smalley, R. E.; Weisman, R. B. *Science* **2002**, *298*, 2361.